

# Model Predictive Controlled IM Drive based on IT2FNN Controller

Research paper

Ridvan Demir<sup>1,\*</sup>, Recep Yildiz<sup>2</sup>, Ahmet Gani<sup>1</sup><sup>1</sup>Department of Electrical and Electronics Engineering, Kayseri University, Kayseri, Türkiye<sup>2</sup>Department of Electrical and Electronic Engineering, Nigde Omer Halisdemir University, Nigde, Türkiye

Received: 23 September, 2023; Accepted: 25 October, 2023

**Abstract:** In this paper, the predictive torque control (PTC) based induction motor (IM) drive using an interval type-2 fuzzy neural network (IT2FNN) controller in the speed control loop is designed and tested in simulations. The states required for the proposed motor drive are estimated by extended complex Kalman filter (ECKF). The ECKF performs online estimations of stator currents, rotor fluxes, rotor mechanical speed, and rotor resistance. Compared to conventional extended Kalman filter (EKF), which estimates the same states/parameters, the designed ECKF has less computational burden because it does not contain matrix inverse and the matrix dimensions have been reduced. In addition, the rotor resistance estimated by ECKF is updated online to the PTC system. Thus, the performance of the PTC-based IM drive is improved against variations in the rotor resistance, whose value changes with operating conditions such as frequency and temperature. In order to force both the ECKF observer and the proposed IM drive, a challenging scenario containing the wide speed range operation of the IM is designed. Simulation results confirm the performance of the proposed speed-sensorless PTC-based drive that uses an IT2FNN controller in the speed control loop and the estimation performance of the ECKF observer.

**Keywords:** induction motor • extended complex Kalman filter • predictive torque control • IT2FNN • speed-sensorless motor drive

## 1. Introduction

Induction motors (IMs) have been widely used in electrical vehicles and industrial applications that require varying torque or speed control on account of their characteristic advantages such as low cost, reliability, and high durability. The performances of IM drives have increased with the introduction of vector control-based methods such as the field oriented control (FOC) and direct torque control (DTC) systems. High-performance speed-sensorless IM drives based on FOC, DTC, and predictive torque control (PTC) require a controller for the speed control loop and a speed observer or estimator to eliminate the need for a speed sensor. Considering the high-performance control application of IM, the PTC method does not need proportional-integral (PI) current controllers (for FOC) or hysteresis comparators (for DTC), coordinate transformation, and PWM technique as stated in Wang et al. (2018). In addition, model predictive control (MPC) that combines the advantages, such as easy implementation and dynamic response, is introduced for IM drive (Rodriguez et al., 2012; Wang et al., 2018). The main MPC strategies for IM control applications can be classified as the predictive current control (PCC) (Mousavi et al., 2021) and PTC (Mousavi et al., 2023). In order to obtain torque reference in the PTC and stator current reference in the PCC method, the PI controller is used in the external speed control loop. However, PI controllers are generally sensitive against the operating conditions of IM. Therefore, there is a requirement for controller structures that are less sensitive to rotor mechanical speed, motor parameters, and load torque changes (Sabzalian et al., 2020). In order to increase the control performance of IMs, many intelligent controller structures instead of conventional

\* Email: ridvandemir@kayseri.edu.tr

PI have been proposed in the literature. In Mencou et al. (2023), to overcome the limitations of the PI controller used in speed control loop conventional DTC-based IM drives, the fuzzy logic (FL) speed controller is designed. In Kamalapur and Aspalli (2023), a fractional-order fuzzy logic controller (FLC) instead of the PI controller is proposed in the speed control loop, in order to improve the control performance of the DTC-based IM drive. In Elmorshedy et al. (2020), a FLC is proposed for the speed control loop of the predictive thrust control system for linear IM. Ayodhya et al. (2022) present a comparative analysis of the conventional PI and FLC-based speed controllers for indirect vector-controlled IM drives. In Acikgoz (2020), to obtain improved speed response from IM, a type-2 fuzzy neural network (T2FNN) controller is designed. In Prasad and Durgasukuamar (2021), a T2FNN controller for the vector control-based IM drive is proposed. It has been shown that the control performance of the T2FNN controller is higher than that of the conventional PI and type-1 fuzzy neural network (T1FNN) controllers in both Acikgoz (2020) and Prasad and Durgasukuamar (2021).

Along with the need for measured rotor speed information for PTC in the external speed control loop, its measurement causes cost, hardware complexity, and maintenance requirement. Therefore, instead of measuring the rotor speed, various model-based observers/estimators, increasing the reliability of the IM drive, have been proposed for speed-sensorless control in the literature. These estimators/observers can be classified as reduced/full-order observers (Orlowska-Kowalska et al., 2019), sliding-mode observer (Mousavi et al., 2023), model reference adaptive systems (Das et al., 2019), extended Luenberger observers (You et al., 2018), and unscented/extended Kalman filters (EKF) (Yildiz et al., 2020). Contrary to the other methods, the EKFs offer a stochastic approach taking into account the measurement and system noises for the states and parameters estimations of IM (Demir, 2023). Therefore, many researchers use the EKF algorithm to realise state and parameter estimations of nonlinear systems in the literature. Looking at the state and parameter estimation method, Kalman filter based methods present high accuracy for state and parameter estimation of IM. On the other hand, Kalman filter based methods can be classified as being associated with a high computational burden, as stated in Bednarz and Dybkowski (2019).

Taking into account the studies using the EKF to estimate the states and parameters of the IM, stator stationary axis components of rotor fluxes ( $\varphi_{r\alpha}$  and  $\varphi_{r\beta}$ ), rotor mechanical speed ( $\omega_m$ ), and rotor resistance ( $R_r$ ) are estimated by conventional EKF in Altinisik and Demir (2021). In Zerdali and Demir (2021),  $i_{s\alpha}$ ,  $i_{s\beta}$ ,  $\varphi_{r\alpha}$ ,  $\varphi_{r\beta}$ ,  $\omega_m$ , and load torque ( $\tau_l$ ) estimations are realised by using EKF algorithm. Moreover, extended complex Kalman filters (ECKFs) have been proposed in the literature to reduce the computational burden of the conventional EKF used in state and parameter estimations of IM (Alonge et al., 2014; Zerdali, 2018). To perform air gap flux oriented control of IM, Menaa et al. (2008) presents an ECKF to perform online estimations of air gap fluxes, rotor mechanical speed, rotor resistances, and mutual inductance by using measured stator currents. Alonge et al. (2014) introduce the estimations of the  $i_{s\alpha}$ ,  $i_{s\beta}$ ,  $\varphi_{r\alpha}$ ,  $\varphi_{r\beta}$ , and  $\omega_m$  with the ECKF algorithm. In addition to the states estimated by Alonge et al. (2014),  $t_L$  estimation is carried out with the ECKF algorithm in Zerdali (2018).

The main contribution of this study lies in its proposal of a PTC-based IM drive using a T2FNN controller in the speed control loop to avoid the performance deteriorations associated with the conventional PI. For this aim, the states required for the proposed motor drive are estimated by ECKF algorithm. The ECKF observer performs online estimations of  $i_{s\alpha}$ ,  $i_{s\beta}$ ,  $\varphi_{r\alpha}$ ,  $\varphi_{r\beta}$ ,  $\omega_m$ , and  $R_r$ . Compared to conventional EKF (Altinisik and Demir, 2021), which estimates the same states/parameters, the designed ECKF has less computational burden because it does not contain matrix inverse and the matrix dimensions are reduced. Another motivation for this study is to improve the performance of the PTC-based IM drive against the  $R_r$  changes by estimating and thus updating its frequency and temperature based variations in both ECKF observer and the proposed IM drive.

The section above has provided a literature review on speed-sensorless model-based estimation and control methods of IMs. The remainder of this paper is organised as follows: Section 2 presents the details of the extended complex mathematical model of IM, Section 3 the design of ECKF observer using extended complex IM model, Section 4 details of the interval type-2 fuzzy neural network (IT2FNN) controller, Section 5 the proposed speed-sensorless PTC system, Section 6 simulation studies, and Section 7 the study's conclusions.

## 2. Complex Mathematical Model of IM

The state space representation of the complex dynamic IM model is given in Eqs (1) and (2) in continuous form. In this paper, the conventional rotor flux based infinite inertia model of IM is extended by an additional state, which is  $R_r$ .

$$\begin{aligned}\dot{\mathbf{x}}_t &= \mathbf{f}(\mathbf{x}_t, \mathbf{u}_t) + \mathbf{w} \\ \dot{\mathbf{x}}_t &= \mathbf{A}(\mathbf{x}_t)\mathbf{x}_t + \mathbf{B}\mathbf{u}_t + \mathbf{w}\end{aligned}\quad (1)$$

$$\begin{aligned}\mathbf{z}_t &= \mathbf{h}(\mathbf{x}_t) + \mathbf{v} \\ \mathbf{z}_t &= \mathbf{H}\mathbf{x}_t + \mathbf{v}\end{aligned}\quad (2)$$

where the extended complex state vector is  $\mathbf{x}_t = [x_1, x_2, x_3, x_4]^T = [i_{s\alpha} + ji_{s\beta}, \varphi_{r\alpha} + j\varphi_{r\beta}, \omega_m, R_r]^T$ . The complex input is  $\mathbf{u}_t = u_s = [u_{s\alpha} + ju_{s\beta}]$ . The complex measurement is  $\mathbf{z}_t = [i_{s\alpha} + ji_{s\beta}]$ . The function of outputs is  $h(\mathbf{x}_t)$ . The measurement vector is  $\mathbf{H} = [1 \ 0 \ 0 \ 0]$ .  $\mathbf{A}$  and  $\mathbf{B}$  are the extended system and control input matrix, respectively. The measurement and process noises are referred to, respectively, by  $\mathbf{v}$  and  $\mathbf{w}$  in state space representation, and both of these are assumed to be zero mean. Here, the system function  $f(\mathbf{x}_t, \mathbf{u}_t)$  is presented in Eq. (3).

$$f(\mathbf{x}_t, \mathbf{u}_t) = \begin{bmatrix} -\left(\frac{R_s}{L_\sigma} + \frac{R_r L_m^2}{L_\sigma L_r^2}\right)x_1 + \left(\frac{R_r L_m}{L_\sigma L_r} - j\frac{L_m P_p}{L_\sigma L_r}\right)x_3 x_2 + \frac{1}{L_\sigma}u_s \\ \frac{R_r L_m}{L_r}x_1 + \left(\frac{R_r}{L_r} - jp_p x_3\right)x_2 \\ 0 \\ 0 \end{bmatrix}\quad (3)$$

where  $L_\sigma = L_s - L_m^2 / L_r$  represents stator transient inductance;  $L_r$  is the rotor inductance;  $L_s$  is the stator inductance;  $L_m$  is the mutual inductance;  $u_{s\alpha}$  and  $u_{s\beta}$  represent the stator stationary axis ( $\alpha\beta$ -axis) components of stator voltages, respectively;  $P_p$  is the number of pole pairs;  $i_{s\alpha}$  and  $i_{s\beta}$  are the  $\alpha\beta$ -axis components of stator currents;  $\varphi_{r\alpha}$  and  $\varphi_{r\beta}$  are the  $\alpha\beta$ -axis components of rotor fluxes;  $\omega_m$  is the rotor mechanical speed; and  $R_s$  and  $R_r$  are the stator and rotor resistances, respectively.

The discretised IM model is derived from the extended complex IM model given in Eq. (1) with the help of the forward Euler approach given in Eq. (4). Thus, it is possible to use the discretised IM model in the discrete ECKF to perform online estimations. The discrete IM is shown in Eq. (5), where  $T$  refers to the sampling time and  $\mathbf{I}$  refers to the identity matrix.

$$\dot{\mathbf{x}}_t \approx \frac{\mathbf{x}_{k+1} - \mathbf{x}_k}{T}\quad (4)$$

$$\mathbf{x}_{k+1} = T \times \mathbf{f}(\mathbf{x}_k, \mathbf{u}_k) + \mathbf{I}_{4 \times 4} \times \mathbf{x}_k\quad (5)$$

### 3. ECKF

To perform online estimations of  $i_{s\alpha}$ ,  $i_{s\beta}$ ,  $\varphi_{r\alpha}$ ,  $\varphi_{r\beta}$ ,  $\omega_m$ , and  $R_r$  by using ECKF algorithm, the extended complex IM model—the details of which have been presented in Section II—is used in the ECKF observer whose mathematical expressions are given in Eqs (6)–(12) (Alonge et al., 2014). As inferable from Eqs (6)–(12), the ECKF algorithm is similar to the conventional EKF algorithm except for the step in Eq. (8).

$$\mathbf{F}_{k+1|k} = \frac{\partial \mathbf{f}(\mathbf{x}, \mathbf{u})}{\partial \mathbf{x}} \Big|_{\mathbf{x}=\hat{\mathbf{x}}_{k+1}}\quad (6)$$

$$\hat{\mathbf{x}}_{k+1}^- = \mathbf{f}(\hat{\mathbf{x}}_k, \mathbf{u}_{k+1})\quad (7)$$

$$\mathbf{P}_{k+1}^- = \mathbf{F}_{k+1} \mathbf{P}_k \mathbf{F}_{k+1}^H + \mathbf{Q}\quad (8)$$

$$\mathbf{K}_{k+1} = \mathbf{P}_{k+1}^- \mathbf{H}_{k+1}^T [\mathbf{H}_{k+1} \mathbf{P}_{k+1}^- \mathbf{H}_{k+1}^T + \mathbf{R}]^{-1}\quad (9)$$

$$\hat{\mathbf{x}}_{k+1} = \hat{\mathbf{x}}_{k+1}^- + \mathbf{K}_{k+1} (\mathbf{z}_{k+1} - \mathbf{H}_{k+1} \hat{\mathbf{x}}_{k+1}^-)\quad (10)$$

$$\mathbf{P}_{k+1} = \mathbf{P}_{k+1}^- - \mathbf{K}_{k+1} \mathbf{H}_{k+1} \mathbf{P}_{k+1}^- \quad (11)$$

Here,  $F_{k+1|k}$  represents the linearisation function, namely the Jacobian matrix;  $H$  refer to complex conjugate transpose of a matrix;  $P_{k+1}^-$  and  $P_{k+1}$  are the priori and the posteriori estimation error covariance matrices, respectively;  $K_{k+1}$  is the Kalman gain; and  $Q$  and  $R$  are the noise covariance matrices, namely modelling and measurement errors, respectively.

The ECKF observer has computational load advantages compared to the conventional EKF algorithm, as stated in Alonge et al. (2014). The main reasons why the ECKF presents less computational burden can be given as follows:

- Since the complex model of the nonlinear system is used in the ECKF, the matrix dimensions are reduced and thus element-based multiplication operations in ECKF are less than those in the conventional EKF.
- Similar to the conventional EKF,  $P_{k+1}^-$ ,  $P_{k+1}$ ,  $K_{k+1}$ ,  $Q$ , and  $R$  in Eqs (6)–(12) consist of real elements with reduced dimensions due to usage of complex IM model.
- Inverse matrix operation is one of the reasons why the conventional EKF has been classified as a case of high computational burden. As stated above, when applying the ECKF algorithm, the size of the matrix to be inverted is reduced, which leads to decreased computational burden. In this paper, since  $\vec{i}_s = i_s \alpha + j i_s \beta$  vector is the only state that is measured, the result of the mathematical operation in  $H_{k+1} P_{k+1}^- H_{k+1}^T + R$  is a scalar and real value as stated in Alonge et al. (2014). Therefore, the matrix inverse operation in the conventional EKF is converted into the inverse operation of a real number in the ECKF, which requires much less computational burden compared to the matrix inverse.

The complexity of the design process for ECKFs, which reduces the computational burden compared to the conventional EKF algorithm, can be evaluated as the disadvantage of ECKF due to the use of an extended complex IM model.

## 4. IT2FNN based on TSK Logic Model

Type-2 fuzzy logic controller (T2FLC) is an extended version of type-1 fuzzy logic controller (T1FLC) and it deals with numerical and linguistic uncertainties. The membership function (MF) of a general T2FLC is three-dimensional. The principal reason for the proposal of two-dimensional interval T2FLC (IT2FLC) is the ensuring of a reduced degree of computational complexity in comparison with general T2FLC (Acikgoz et al., 2023). Fuzzy neural networks (FNNs) refer to combinations of artificial neural networks (ANNs) and FL. Depending on the use of T1FLC or T2FLC, such controller structures are called T1FNN or T2FNN controllers. These controllers incorporate the superior features of ANN and FL (Acikgoz, 2020). An IT2FNN controller structure having two inputs and one output is used in this study. Inputs of the IT2FNN controller are selected as rotor angular speed error ( $e$ ) and change of this error ( $\Delta e$ ). The structure of IT2FNN used in this study is based on first-order interval type-2 Takagi-Sugeno-Kang (IT2TSK) FL model and is depicted in Figure 1.

As depicted in Figure 1, IT2FNN structure has five layers with two inputs and one output. IT2FNN inferences deploy a set of rules, including interval type-2 MFs to represent linguistic terms. Antecedent parts of the IT2FNN connect interval type-2 fuzzy sets with fixed means and uncertain standard deviation, and the consequent parameters have Takagi-Sugeno-Kang (TSK) type that realises linear equations of input variables with an interval set (Abiyev and Kaynak, 2010). Each rule for IT2FNN can be given as follows (Castro et al., 2009):

$$i^{\text{th}} \text{Rule : IF } x_1 \text{ is } \tilde{A}_1^i \text{ and } x_2 \text{ is } \tilde{A}_2^i \dots \text{ and } x_n \text{ is } \tilde{A}_n^i \text{ then } y_i = \tilde{a}_0^i + \sum_{j=1}^n \tilde{a}_j^i x_j, (i = 1 \dots M) \quad (12)$$

where  $x$  refers to inputs,  $\tilde{A}_j^i$  represents interval fuzzy sets, and  $\tilde{a}_j^i$  represents interval sets.

Layer-1: This layer is called the input layer. It takes inputs having real values.

Layer-2: MFs are determined in each node of this layer and the fuzzification process is executed by using interval type-2 MFs. Gaussian type MFs with fixed mean ( $m_j^i$ ) and uncertain standard deviation ( $\sigma_j^i$ ) are preferred in this study due to their effective result and uncertainty boundary width. Three Gaussian MFs are used for each input. Gaussian MF can be formulated as follows:

$$\mu_{\tilde{A}_j^i} = e^{-\left(\frac{1}{2} \left(\frac{x_j - m_j^i}{\sigma_j^i}\right)^2\right)} \equiv G(m_j^i, \sigma_j^i; x_j), m_j^i \in [m_{j1}^i, m_{j2}^i] \quad (13)$$

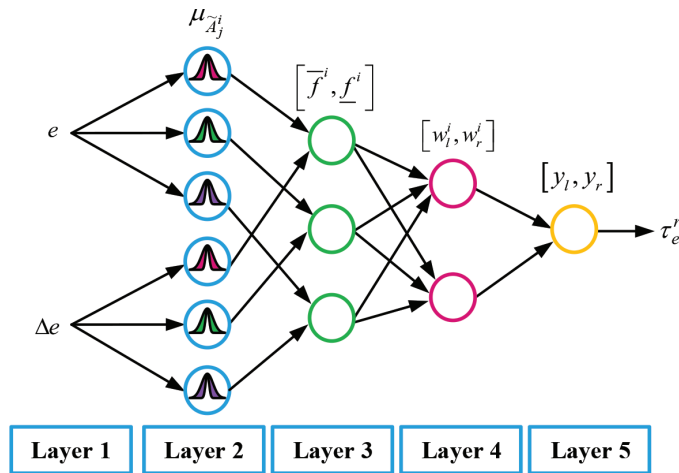


**Fig. 1.** IT2FNN block scheme. IT2FNN, interval type-2 fuzzy neural network.

Layer-3: Each node of Layer-3 represents the antecedent part of a fuzzy rule, and firing strength of each rule is computed in this layer. The calculated firing strength is an interval type-2 fuzzy set and firing strength of the rules for upper and lower boundaries of interval is represented as:  $[\bar{f}^i, f^i]$ . Fuzzy meet operation based on algebraic product operation is performed. The firing strength is calculated as follows:

$$\underline{f}^i = \prod_{j=1}^n \underline{\mu}_j^i, \bar{f}^i = \prod_{j=1}^n \bar{\mu}_j^i \quad (14)$$

Layer-4: This layer is a consequent layer and output of a consequent node in this layer is an interval type-2 set and can be calculated as follows:

$$[w_l^i, w_r^i] = [m_0^i - \sigma_0^i, m_0^i + \sigma_0^i] + \sum_{j=1}^n [m_j^i - \sigma_j^i, m_j^i + \sigma_j^i] x_j \quad (15)$$

The output of Layers 4 and 5 are combined to obtain the output function. The output can be calculated as follows:

$$y_l = \frac{(1-q_l) \sum_{i=1}^M \underline{f}^i w_l^i + q_l \sum_{i=1}^M \bar{f}^i w_l^i}{\sum_{i=1}^M \underline{f}^i + \bar{f}^i} \quad (16)$$

$$y_r = \frac{(1-q_r) \sum_{i=1}^M \bar{f}^i w_r^i + q_r \sum_{i=1}^M \underline{f}^i w_r^i}{\sum_{i=1}^M \underline{f}^i + \bar{f}^i} \quad (17)$$

where  $l$  and  $r$  symbolise the left and right limits, respectively. The parameters of  $q_l$  and  $q_r$  are called distribution factors.

Layer-5: The node in this layer calculates the output variable with the help of defuzzification operation. The following equation gives the defuzzified output (Kayacan et al., 2012):

$$y(= \tau_e^r) = y_l + y_r \quad (18)$$

## 5. Predictive Torque Controlled IM Drive

The block diagram of the proposed speed-sensorless PTC-based IM drive including a T2FNN controller in the external speed control loop is shown in Figure 2. To perform the PTC-based control of IM, the required stator fluxes are obtained by using the estimated rotor fluxes, and the electromagnetic torque reference value is calculated

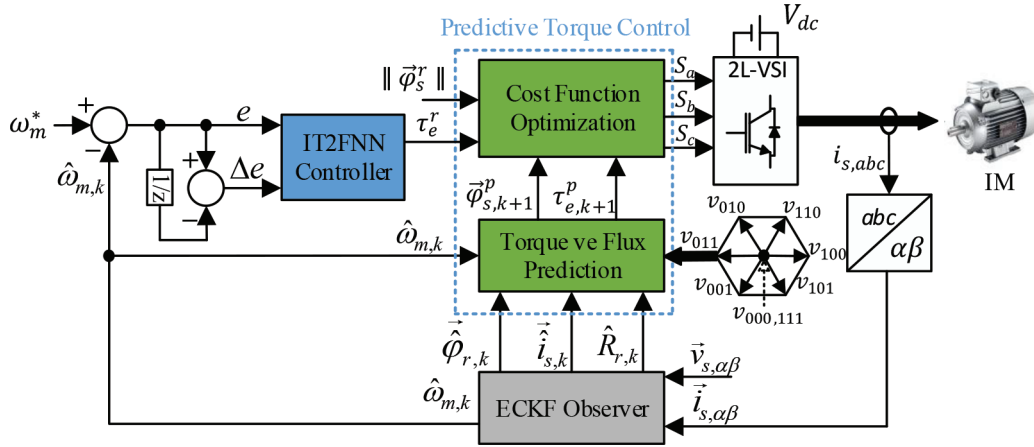


**Fig. 2.** Predictive torque controlled IM drive. IM, induction motor.

according to the difference between the reference and estimated rotor speed values with the help of a T2FNN controller. As indicated in Figure 2, the online estimations of  $i_{s\alpha}$ ,  $i_{s\beta}$ ,  $\varphi_{r\alpha}$ ,  $\varphi_{r\beta}$ ,  $\omega_m$ , and  $R_r$  are performed by using ECKF observer. Therefore, the performance of the speed-sensorless IM drive against parameter changes is increased by updating the estimated  $R_r$  value in the PTC system.

As inferable from Figure 2, the two-level voltage source inverter (2L-VSI) is used in the IM drive. The inverter topology and switching vectors of the 2L-VSI are presented in Figure 3. The switching state and output voltage of the 2L-VSI can be defined as:

$$\vec{S} = \frac{2}{3}(S_a + \bar{a}S_b + \bar{a}^2S_c) \quad (19)$$

$$\vec{v}_s = V_{dc}\vec{S} \quad (20)$$

where  $\bar{a} \triangleq e^{j2\pi/3}$  and  $V_{dc}$  represents the inverter DC link voltage as in Figure 3.

In order to obtain the stator flux vector that is used in the PTC strategy along with electromagnetic torque value to determine the optimal switching state, Eq. (21) is used in this study. As inferable from Eq. (21), the stator flux vector is calculated by using the rotor flux and stator current vectors estimated by ECKF.

$$\vec{\varphi}_{s,k} = \frac{L_m}{L_r}\vec{\varphi}_{r,k} + L_\sigma\vec{i}_{s,k} \quad (21)$$

In the 'torque and flux prediction' block shown in Figure 2, using  $\vec{i}_{s,k}$ ,  $\vec{\varphi}_{s,k}$ , and  $\vec{\varphi}_{r,k}$ , the predicted stator flux and stator current vectors as well as the predicted electromagnetic torque value at time  $k+1$  can be obtained as follows (Habibullah and Lu, 2015):

$$\vec{\varphi}_{s,k+1}^{p(j)} = \vec{\varphi}_{s,k} + T(\vec{v}_{s,k}^{(j)} - R_s\vec{i}_{s,k}), \quad j \in \{0,1,\dots,7\} \quad (22)$$

$$\vec{i}_{s,k+1}^{p(j)} = \left(1 + \frac{T}{T_\sigma}\right)\vec{i}_{s,k} + \frac{T}{T + T_\sigma} \left(\frac{1}{R_\sigma} \left(\frac{k_r}{T_r} - k_r j \hat{\omega}_{r,k}\right) \vec{\varphi}_{r,k} + \vec{v}_{s,k}^{(j)}\right), \quad j \in \{0,1,\dots,7\} \quad (23)$$

$$\tau_{e,k+1}^{p(j)} = \frac{3}{2} p_p \Im m \left\{ \left( \vec{i}_{s,k+1}^{p(j)} \right) \left( \vec{\varphi}_{s,k+1}^{p(j)} \right)^* \right\}, \quad j \in \{0,1,\dots,7\} \quad (24)$$

where  $R_\sigma = R_s + k_r^2 \hat{R}_r$ ,  $T_\sigma = L_\sigma / R_\sigma$ ,  $T_r = L_r / \hat{R}_r$ ,  $k_r = L_m / L_r$ , and  $\omega_r = p_p \hat{\omega}_m$ .

Finally, Eq. (25) presents the predefined cost function to acquire the optimal switching vector. As inferable from Eq. (25), the reference and predicted values of stator flux and electromagnetic torque for all switching states are

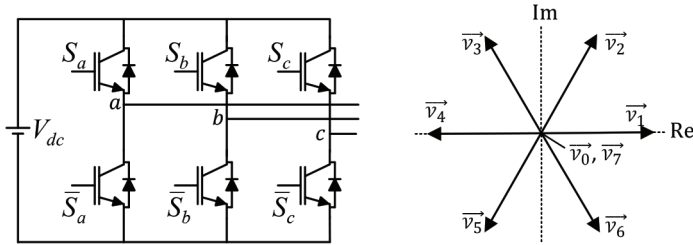


**Fig. 3.** 2L-VSI and voltage vectors. 2L-VSI, two-level voltage source inverter.

applied to the cost function. Hence, the optimum voltage vector minimising the cost function is selected as the next switching state of the inverter (Zerdali and Demir, 2021).

$$g = \sum_{h=1}^N \left\{ \left| \tau_e^r - \tau_{e,k+h}^{p(j)} \right| + \gamma \left| \bar{\varphi}_s^r - \left| \bar{\varphi}_{s,k+h}^{p(j)} \right| \right| + I_{m,k+h} \right\} \quad (25)$$

where  $\gamma$  refers to the weighting factor of the stator flux error. The prediction horizon ( $N$ ) is chosen as 1 in this study.  $I_m$  is the overcurrent protection term that is used to block the selection of a switching state resulting in overcurrent flow in stator windings of the IM and is given in Eq. (26).

$$I_{m,k+h} = \begin{cases} 0, & \text{if } \left| \bar{i}_{s,k+1}^{-p} \right| \leq i_{s,max} \\ \infty, & \text{if } \left| \bar{i}_{s,k+1}^{-p} \right| > i_{s,max} \end{cases} \quad (26)$$

## 6. Simulations

To approve the effectiveness of the proposed PTC-based IM drive using an IT2FNN controller in the speed control loop as in Figure 2, it is implemented and tested in Matlab/Simulink (MathWorks, 2023). In order to make the simulation studies compatible with the one performed before (Altinisik and Demir, 2021), the sampling time ( $T$ ) is chosen as  $25\mu s$ . The parameters and rated values of the three-phase IM used in simulations are presented in Table 1. So as to decrease the computational burden, the initial error covariance matrix ( $P_0$ ),  $Q$ , and  $R$  are selected as diagonal in ECKF observer, and their values are determined by trial and error as follows:

$$P_0 = \text{diag}\{1 \quad 1 \quad 1\}$$

$$R = [10^{-12}]$$

$$Q = \text{diag}\{10^{-8} \quad 10^{-12} \quad 10^{-2} \quad 10^{-4}\}$$

In order to force both the ECKF observer and the proposed IM drive, challenging scenarios containing the wide speed range operation of the IM are designed. In the first scenario,  $\tau_l$  and  $R_r$  parameters are varied step-like or linearly over a wide speed range. In the second scenario, speed is varied step-like from zero speed to rated speed. Therefore, with this challenging scenario, it is aimed to test both the estimation performance of the ECKF and the robustness of the proposed IM drive under the cases of temperature and frequency based  $R_r$  variations and unknown mechanical inputs causing  $\tau_l$  changes. The estimation results for the ECKF observer and the tracking performance of the proposed drive system are presented in Figures 4 and 6. In addition, the estimation errors related to the ECKF are given in Figures 5 and 7. Here in Figures 4-7, ' $r$ ' refers to reference values, and ' $m$ ' and ' $est$ ' indicate measured and estimated states, respectively. Also, ' $e_{(.)}$ ' indicates the estimation error defined as the difference between the measured and the estimated values.

$P$ [kW]	$V$ [V]	$I$ [A]	$f$ [Hz]
3	380	6.9	50
$R_s$ [ $\Omega$ ]	$R_r$ [ $\Omega$ ]	$L_m$ [H]	$L_r = L_s$ [H]
2.283	2.133	0.22	0.2311
$p_p$	$n_{mn}$ [r/min]	$\tau_l$ [Nm]	
2	1,430	20	

IM, induction motor.

**Table 1.** IM parameters.

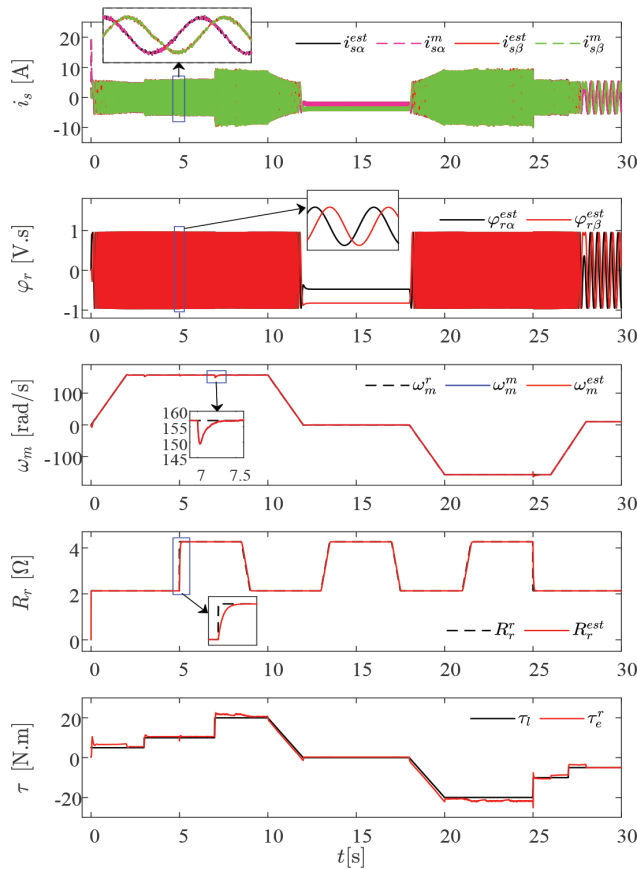


**Fig. 4.** Tracking robustness of the proposed IM drive and estimation performance of the ECKF for the wide speed range scenario. ECKF, extended complex Kalman filter; IM, induction motor.

In this study, the computational burden of the conventional EKF in Altinisik and Demir (2021) and ECKF in this study, which estimate the same states and parameters, are compared. For the scenario given in Figure 4, each observer is operated 50 times under the same conditions and the average simulation times obtained by tic-toc command of Matlab are given in Table 2.

After presenting the simulation results related to ECKF and the proposed IM drive, it is possible to deduce the following inferences in light of Figures 4–7 and Table 2:

- It is clear that highly impressive estimation performance is achieved by using the ECKF observer against the challenging scenarios in simulations. Therefore, with the help of performing online estimations of  $i_{s\alpha}$ ,  $i_{s\beta}$ ,  $\varphi_{r\alpha}$ ,  $\varphi_{r\beta}$ ,  $\omega_m$ , and  $R_r$  in a successful manner, robust tracking performance is obtained from the proposed PTC-based IM drive with IT2FNN controller in the external speed control loop.

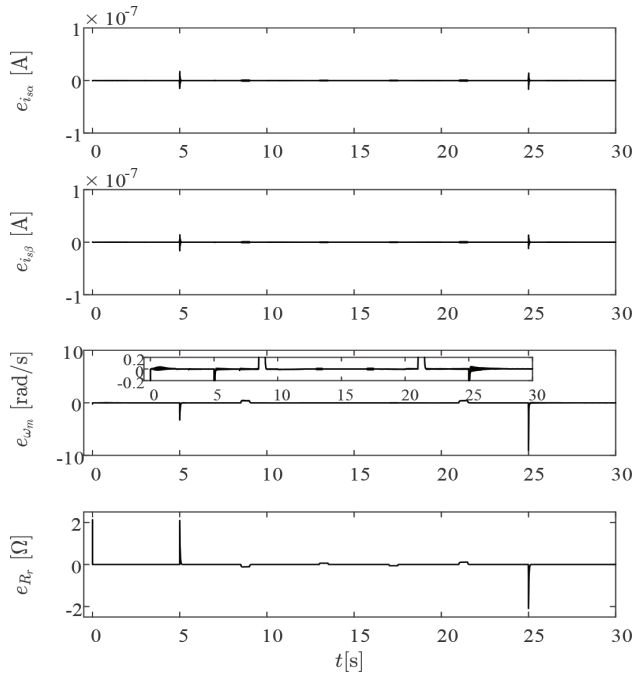


**Fig. 5.** Resulting estimation errors for ECKF in the wide speed range scenario. ECKF, extended complex Kalman filter.

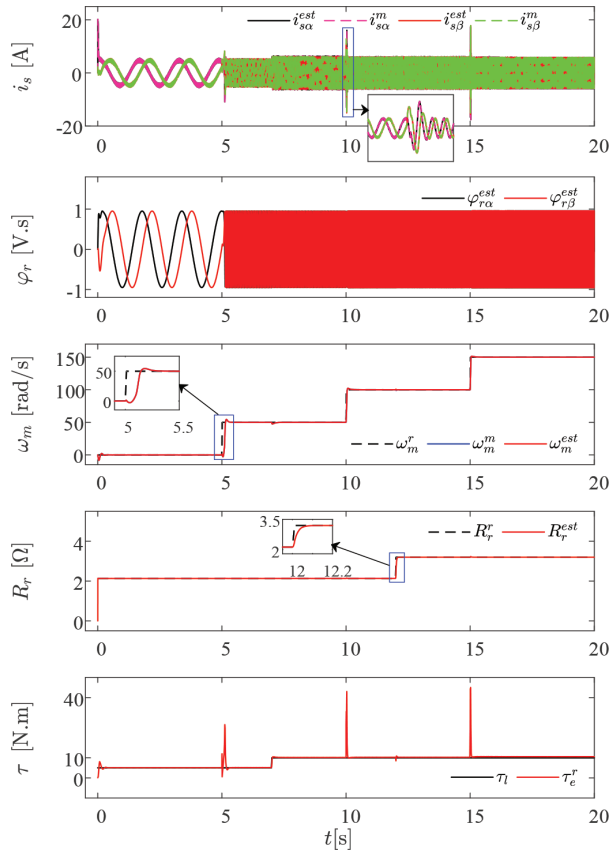


**Fig. 6.** Tracking robustness of the proposed IM drive and estimation performance of the ECKF for different step-like speed references. ECKF, extended complex Kalman filter; IM, induction motor.

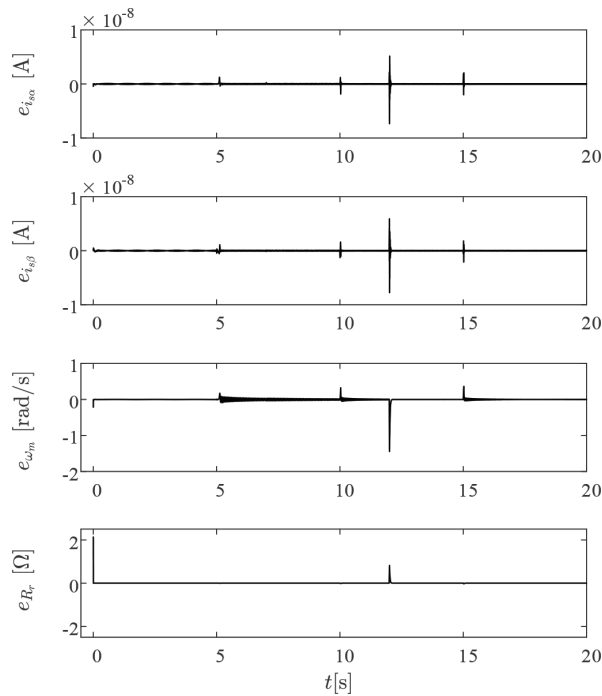


**Fig. 7.** Resulting estimation errors for ECKF in the different step-like speed references. ECKF, extended complex Kalman filter.

Conventional EKF (Altinisik and Demir, 2021)	ECKF
27.5272 s	23.1925 s

ECKF, extended complex Kalman filter; EKF, extended Kalman filter.

**Table 2.** The computational times of the ECKF and conventional EKF (Altinisik and Demir, 2021).

- Although the ECKF observer is operated with zero initial values for all estimated states and parameters, these estimated values converge to their real values in a short period of time. Moreover, to make the test scenario more challenging, the DC condition is also tested. However, the proposed IM drive performance easily handles this difficulty, as presented in Figure 4.
- As given in Table 2, a computational burden comparison is carried out between the conventional EKF and ECKF algorithms in the case of performing the estimations of the same states and parameters. Since the ECKF algorithm utilises the extended complex IM model causing reduced matrix dimension and elimination of matrix inverse process, the average simulation time for the ECKF observer is approximately 15.75% shorter than that of the conventional EKF.

In summary, simulation results confirm the performance of the speed-sensorless PTC-based drive that uses an IT2FNN controller in the speed control loop and the estimation performance of the ECKF observer.

## 7. Conclusions

In this paper, the PTC-based IM drive using an IT2FNN controller in the external speed control loop is designed and tested in simulations. The states ( $i_{s\alpha}$ ,  $i_{s\beta}$ ,  $\varphi_{r\alpha}$ ,  $\varphi_{r\beta}$ , and  $\omega_m$ ) required for the proposed motor drive are estimated by ECKF. Furthermore, the  $R_r$  is estimated by ECKF to be updated simultaneously in the PTC system. Thus, the performance of the PTC-based IM drive is improved against the  $R_r$ , whose value changes with operating conditions such as frequency and temperature. Simulation results confirm the performance of the speed-sensorless PTC-based drive and the estimation performance of the ECKF observer. In addition, the computational burden of the

ECKF observer is compared with that of the conventional EKF, with the latter of these estimating the same state and parameters, and this comparison demonstrates that the computational burden decreased by approximately 15.75%. Future studies will focus on real-time experiments of the proposed PTC-based drive system.

## Acknowledgments

This work has been supported by Kayseri University Scientific Research Projects Coordination Unit under grant number FKB-2022-1082.

## References

- Abiyev, R. H. and Kaynak, O. (2010). Type 2 Fuzzy Neural Structure for Identification and Control of Time-Varying Plants. *IEEE Transactions on Industrial Electronics*, 57(12), pp. 4147–4159. doi: 10.1109/TIE.2010.2043036.
- Acikgoz, H. (2020). Real-Time Adaptive Speed Control of Vector-Controlled Induction Motor Drive Based on Online-Trained Type-2 Fuzzy Neural Network Controller. *International Transactions on Electrical Energy Systems*, 30(12), pp. 1–17. doi: 10.1002/2050-7038.12678.
- Acikgoz, H., Coteli, R., Tanyildizi, E., Dandil, B. and Kayisli, K. (2023). Advanced Control of Three-Phase PWM Rectifier Using Interval Type-2 Fuzzy Neural Network Optimized by Modified Golden Sine Algorithm. *Electric Power Components and Systems*, 51(10), pp. 933–948. doi: 10.1080/15325008.2023.2185838.
- Alonge, F., D'Ippolito, F., Fagiolini, A. and Sferlazza, A. (2014). Extended Complex Kalman Filter for Sensorless Control of an Induction Motor. *Control Engineering Practice*, 27, pp. 1–10. doi: 10.1016/j.conengprac.2014.02.007.
- Altinisik, Y. E. and Demir, R. (2021). EKF Based Model Predictive Torque Control of Induction Motors. *European Journal Science and Technology*, 38, pp. 858–863.
- Ayodhya, A., Angadi, S. and Raju, A. B. (2022). Comparative analysis of PI and fuzzy based speed controllers for indirect field-oriented control of induction motor drives. In: *2022 IEEE International Conference on Electronics, Computing and Communication Technologies (CONECCT)*, Bangalore, India, pp. 1–6.
- Bednarz, S. A. and Dybkowski, M. (2019). Estimation of the Induction Motor Stator and Rotor Resistance Using Active and Reactive Power Based Model Reference Adaptive System Estimator. *Applied Sciences*, 9(23), p. 5145. doi: 10.3390/app9235145.
- Castro, J. R., Castillo, O., Melin, P. and Rodríguez-Díaz, A. (2009). A Hybrid Learning Algorithm for a Class of Interval Type-2 Fuzzy Neural Networks. *Information Sciences Special Section on High Order Fuzzy Sets*, 179(13), pp. 2175–2193.
- Das, S., Kumar, R. and Pal, A. (2019). MRAS Based Speed Estimation of Induction Motor Drive Utilizing Machine's d- and q- Circuit Impedances. *IEEE Transactions on Industrial Electronics*, 66(6), pp. 4286–4295. doi: 10.1109/TIE.2018.2860530.
- Demir, R. (2023). Robust Stator Flux and Load Torque Estimations for Induction Motor Drives with EKF-Based Observer. *Electrical Engineering*, 105, pp. 551–562. doi: 10.1007/s00202-022-01717-y.
- Elmorshedy, M. F., Xu, W., Ali, M. M., Liu, Y. and Allam, S. M. (2020). High performance speed sensorless finite-set predictive thrust control of a linear induction motor based on MRAS and fuzzy logic controller. In: *2020 IEEE 9th International Power Electronics and Motion Control Conference (IPEMC2020-ECCE Asia)*, Nanjing, China, pp. 3039–3044.
- Habibullah, M. and Lu, D. D. C. (2015). A Speed-Sensorless FS-PTC of Induction Motors Using Extended Kalman Filters. *IEEE Transactions on Industrial Electronics*, 62(11), pp. 6765–6778. doi: 10.1109/TIE.2015.2442525.
- Kamalapur, G. and Aspalli, M. S. (2023). Direct Torque Control and Dynamic Performance of Induction Motor Using Fractional Order Fuzzy Logic Controller. *International Journal of Electrical and Computer Engineering*, 13(4), pp. 3805–3816. doi: 10.11591/ijece.v13i4.pp3805-3816.
- Kayacan, E., Cigdem, O. and Kaynak, O. (2012). Sliding Mode Control Approach For Online Learning as Applied To Type-2 Fuzzy Neural Networks And Its Experimental Evaluation. *IEEE Transactions on Industrial Electronics*, 59(9), pp. 3510–3520. doi: 10.1109/TIE.2011.2182017.

- MathWorks Inc. (2023). *Simulink. Simulation and Model-Based Design*. MA, USA: Natick.
- Menaa, M., Touhami, O., Ibtouen, R. and Fadel, M. (2008). Sensorless Direct Vector Control of an Induction Motor. *Control Engineering Practice*, 16(1), pp. 67–77. doi: 10.1016/j.conengprac.2007.04.002.
- Mencou, S., Yakhlef, M. B. and Tazi, E. B. (2023). Fuzzy logic speed controller for robust direct torque control of induction motor drives. In: S. Motahhir, B. Bossoufi, eds., *Digital Technologies and Applications, Lecture Notes in Networks and Systems*. Cham: Springer Nature Switzerland, pp. 601–611.
- Mousavi, M. S., Davari, S. A., Nekoukar, V., Garcia, C., He, L., Wang, F. and Rodriguez, J. (2023). Predictive Torque Control of Induction Motor Based on a Robust Integral Sliding Mode Observer. *IEEE Transactions on Industrial Electronics*, 70(3), pp. 2339–2350. doi: 10.1109/TIE.2022.3169831.
- Mousavi, M. S., Davari, S. A., Nekoukar, V., Garcia, C. and Rodriguez, J. (2021). Finite-Set Model Predictive Current Control of Induction Motors by Direct Use of Total Disturbance. *IEEE Access*, 9, pp. 107779–107790. doi: 10.1109/ACCESS.2021.3100506.
- Orlowska-Kowalska, T., Korzonek, M. and Tarchala, G. (2019). Stability Improvement Methods of the Adaptive Full-Order Observer for Sensorless Induction Motor Drive-Comparative Study. *IEEE Transactions on Industrial Informatics*, 15(11), pp. 6114–6126. doi: 10.1109/TII.2019.2930465.
- Prasad, R. R. and Durgasukumar, G. (2021). Performance Analysis of PI, T1NFC, and T2NFC of Indirect Vector Control-Based Induction Motor Using DSpace-2812. *Journal Européen des Systèmes Automatisés*, 54, pp. 671–682. doi: 10.18280/jesa.540502.
- Rodriguez, J., Kennel, R. M., Espinoza, J. R., Trincado, M., Silva, C. A. and Rojas, C. A. (2012). High-Performance Control Strategies for Electrical Drives: An Experimental Assessment. *IEEE Transactions on Industrial Electronics*, 59(2), pp. 812–820. doi: 10.1109/TIE.2011.2158778.
- Sabzalian, M. H., Mohammadzadeh, A., Lin, S. and Zhang, W. (2020). A Robust Control of A Class of Induction Motors Using Rough Type-2 Fuzzy Neural Networks. *Soft Computing*, 24, pp. 9809–9819. doi: 10.1007/s00500-019-04493-3.
- Wang, F., Zhang, Z., Mei, X., Rodríguez, J. and Kennel, R. (2018). Advanced Control Strategies of Induction Machine: Field Oriented Control, Direct Torque Control and Model Predictive Control. *Energies*, 11(1), 120.
- Yildiz, R., Barut, M. and Zerdali, E. (2020). A Comprehensive Comparison of Extended and Unscented Kalman Filters for Speed-Sensorless Control Applications of Induction Motors. *IEEE Transactions on Industrial Informatics*, 16(10), pp. 6423–6432. doi: 10.1109/TII.2020.2964876.
- You, J., Wu, W. and Wang, Y. (2018). An Adaptive Luenberger Observer for Speed-Sensorless Estimation of Induction Machines. In: 2018 Annual American Control Conference (ACC), Milwaukee, WI, USA, pp. 307–312. doi: 10.23919/ACC.2018.8431006.
- Zerdali, E. (2018). The Design of Extended Complex Kalman Filter Based Speed Sensorless Induction Motor Drive. *Gazi University Science Journal: Part: C Design and Technology*, 6(4), pp. 877–886.
- Zerdali, E. and Demir, R. (2021). Speed-Sensorless Predictive Torque Controlled Induction Motor Drive with Feed-Forward Control of Load Torque for Electric Vehicle Applications. *Turkish Journal of Electrical Engineering and Computer Sciences*, 29(1), pp. 223–240. doi: 10.3906/elk-2005-75.